

Shear and transport in a flow environment determine spatial patterns and population dynamics in a model of nonlocal ecological competition.

Nathan O. Silvano^{1,2}, João Valeriano^{3,4}, Emilio Hernández-García⁵, Cristóbal López⁵, and Ricardo Martínez-García^{*1,4}

¹Center for Advanced Systems Understanding (CASUS) – Helmholtz-Zentrum Dresden-Rossendorf (HZDR), Görlitz, Germany

²Departamento de Física Teórica, Universidade do Estado do Rio de Janeiro, Rio de Janeiro, RJ, Brazil.

³Turing Center for Living Systems, Aix-Marseille University, CNRS, CINAM, Marseille, France

⁴ICTP South American Institute for Fundamental Research & Instituto de Física Teórica, Universidade Estadual Paulista - UNESP, São Paulo SP, Brazil

⁵Institute for Cross-Disciplinary Physics and Complex Systems (IFISC), CSIC-UIB, Palma de Mallorca, Spain

Abstract

Populations very often self-organize into regular spatial patterns with important ecological and evolutionary consequences. Yet, most existing models neglect the effect that external biophysical drivers might have both on pattern formation and the spatiotemporal population dynamics once patterns form. Here, we investigate the effect of environmental flows on pattern formation and population dynamics using a spatially nonlocal logistic model (or Fisher-Kolmogorov equation) coupled to a simple shear and a Rankine vortex flow. We find that, whereas population abundance generally decreases with increasing flow intensity, the effect of the flow on the pattern instability depends on the spatial structure of the flow velocity field. This result shows that the velocity field interacts with the spatial feedbacks responsible for pattern formation in non-trivial ways, leading to a variety of spatiotemporal population dynamics regimes in which the total population abundance can exhibit either regular oscillations with a characteristic frequency or more erratic dynamics without a well-defined period. More generally, the diversity of spatiotemporal population dynamics caused by the interplay between self-organizing feedbacks and environmental flows highlights the importance of incorporating environmental and biophysical processes when studying both ecological pattern formation and its consequences.

*Corresponding author: r.martinez-garcia@hzdr.de

1 Introduction

Populations very often form self-organized spatial patterns caused by nonlinear interactions among organisms and between organisms and their environment [1]. Examples of these patterns appear on a broad range of observational scales, from cell populations to landscapes [2–5], and both in marine and terrestrial environments [6–8]. Across this variety of systems, patterns often impact several ecological processes such as population growth and extinction [9–11], species interactions [12–15], or evolutionary dynamics [16, 17]. A lot of research has therefore focused on understanding, mainly using theoretical models, how different feedbacks between processes controlling population growth and movement affect pattern formation and their system-level ecological and evolutionary consequences [1, 6].

Most of these studies assume that organisms move randomly, either with constant or density-dependent diffusion [18–21], or exhibiting some sort of active movement [22, 23]. Other spatial processes affecting population mixing, such as those induced by environmental flows in aqueous environments, also have important ecological and evolutionary consequences. For example, planktonic microorganisms live in environments where rapidly changing flow velocities can create different levels of population mixing [24–26] and impact encounter rates [27]. This dependence of the encounter rates on flow properties has important consequences for population growth [28, 29] and patchiness [30], determines the outcome of species interactions [31, 32] and might promote the fixation of traits that would get lost in uniform environments [33–35]. In wave-exposed coastal populations, such as mussel or seagrass beds, environmental variability due to cyclic tides and marine currents shapes pattern structure and makes these populations more resistant to long-term environmental shifts [20, 36]. Environmental flows, therefore, play an important role both in determining population spatial structure and their long-term dynamics.

Most studies on the influence of flows on pattern formation in ecological systems have considered individual-based models in which the population is described by a collection of interacting particles [24] or continuous models based on partial differential equations for a population density field in which patterns form due to Turing or differential-flow instabilities [37, 38]. As representative of a different mechanism for pattern formation in continuous models, the nonlocal logistic model (or nonlocal Fisher-Kolmogorov equation), which assumes only diffusive dispersal and exponential population growth limited by long-range intraspecific competition, is one of the simplest population-dynamics models exhibiting pattern formation [39–43]. With this minimum set of processes, patterns of population density can form in the low-diffusion regime if the intensity of the intraspecific competition between two organisms decays sharply enough with the distance between them (or, in mathematical terms, if the Fourier transform of the function that defines this dependence of

the competition strength with the distance between individuals is negative for some wavenumbers [44, 45]). In these conditions, nonlocal interactions can establish regions of very intense competition far from clumps of organisms that destabilize a uniform distribution of population density and lead to the formation of periodic patterns [44–46]. Because of the simple mechanism it proposes to explain pattern formation, the nonlocal logistic model has been the basis for developing more elaborated pattern-formation models testing the effect of additional processes in the spatiotemporal population dynamics, such as demographic fluctuations or environmental heterogeneity [11, 47–49].

Among these extensions, previous work coupled a chaotic flow to an individual-based formulation of the nonlocal logistic model [44]. Keeping all other demographic parameters constant, this study found that increasing mixing first breaks the spotted pattern into non-stationary filaments and, if it continues to increase, takes the population to a well-mixed configuration. Across this gradient of mixing intensity, the stationary population size decreases monotonically. However, these results are obtained only via numerical simulations because the complexity of the chaotic flow and the discreteness of the model make any analytical treatment impossible. Here, we use a continuous description of the nonlocal logistic model and focus on steady flows. These choices, which neglect demographic fluctuations and consider simpler shear and transport dynamics, allow us to go beyond numerical simulations and develop analytical approximations to isolate the key effects of flows on the pattern formation instability and remove fluctuations from the time series of population abundance, thus enabling a simple identification of how flows impact population dynamics.

We consider two flows. First, a sine flow that provides a simple velocity field exhibiting the same properties as parabolic flows in confined channels. This flow mimics, for example, the biophysical environment experienced by microbial populations in pipes where they are subject to anisotropic advective transport and shear forces [32]. Second, we study a vortex flow with closed streamlines and shear forces that are not aligned with any of the primitive vectors of the population pattern [50–52]. For each of these velocity fields, we measure how the flow changes the spatial pattern of population density and how these changes impact the population dynamics and long-term population abundance. Our findings show that the spatial structures of the pattern and the flow velocity field jointly lead to a rich variety of population dynamics, ranging from oscillations with a well-defined frequency for weak flow and population patterns aligned with the main direction of shear and transport, to seemingly chaotic dynamics when the pattern and the flow have very different spatial structures.

2 Materials and Methods

2.1 The nonlocal logistic model with environmental flows

The nonlocal logistic equation is one of the simplest population dynamics models exhibiting self-organized patterns. It describes the spatiotemporal dynamics of a single species diffusing in space and subjected to density-independent growth (asexual reproduction) limited by long-range intraspecific competition. Under these assumptions, the dynamics of the population density ρ is given by

$$\frac{\partial \rho(\mathbf{x}, t)}{\partial t} = r\rho(\mathbf{x}, t) - \beta\rho(\mathbf{x}, t) \int_S G(\mathbf{x} - \mathbf{y})\rho(\mathbf{y}, t)d\mathbf{y} + D\nabla_x^2\rho(\mathbf{x}, t), \quad (2.1)$$

where D and r are the diffusion constant and the net growth rate, respectively. β modulates the intensity of intraspecific competition, S indicates that the integral is performed over the entire system, a square domain of lateral length L with periodic boundary conditions, and $G(\mathbf{x} - \mathbf{y})$ is the competition kernel that defines how strongly the death rate of organisms at a focal location \mathbf{x} is influenced by the presence of conspecifics at neighbor locations \mathbf{y} . We consider that the intensity of nonlocal competition scales with population density (rather than population abundance), which implies that the competition kernel must be normalized to one. This condition guarantees that Eq. (2.1) becomes the logistic model of population growth if $\rho(\mathbf{x}, t)$ is uniform in space.

Previous work has shown that Eq. (2.1) can exhibit spatially periodic patterns of population density when the Fourier transform of $G(\mathbf{x} - \mathbf{y})$ takes negative values for some wavenumbers [44, 45]. As an example of this situation, we assume that the process underlying long-range competition is isotropic and that two organisms at a distance $|\mathbf{x} - \mathbf{y}|$ will compete with each other with a distance-independent strength provided they are closer than a threshold distance R . Mathematically, these assumptions imply choosing an isotropic top-hat kernel of the form

$$G(\mathbf{x}) = \begin{cases} \frac{1}{\pi R^2} & \text{if } |\mathbf{x}| \leq R, \\ 0 & \text{otherwise.} \end{cases} \quad (2.2)$$

To measure the effect of these emergent patterns on the total population abundance, we use a normalized population abundance $A(t)$ defined by the ratio between the total population size, $\int \rho(x, t)d\mathbf{x}$, and the one without spatial patterns, i.e., the uniform steady solution of Eq. (A.1) multiplied by the system size, rL^2/β .

$$A(t) = \frac{\beta}{rL^2} \int_S \rho(\mathbf{x}, t)d\mathbf{x}. \quad (2.3)$$

We extend the nonlocal logistic model in Eq. (2.1) to introduce the effect of transport by a

stationary flow. For these flows, the velocity field does not change in time and therefore it can be written as $\mathbf{v}(\mathbf{x}, t) = v_0 \mathbf{f}(\mathbf{x})$, where v_0 is the maximum velocity of the field and $\mathbf{f}(\mathbf{x})$ is a vectorial function giving the spatial functional dependence of the velocity field, with maximum magnitude equal to one. Under the additional assumption that the velocity field is incompressible, this additional transport process leads to a model equation

$$\frac{\partial \rho(\mathbf{x}, t)}{\partial t} = r\rho(\mathbf{x}, t) - \beta\rho(\mathbf{x}, t) \int_S G(\mathbf{x} - \mathbf{y})\rho(\mathbf{y}, t)d\mathbf{y} + D\nabla_{\mathbf{x}}^2\rho(\mathbf{x}, t) - v_0\mathbf{f}(\mathbf{x}) \cdot \nabla_{\mathbf{x}}\rho(\mathbf{x}, t), \quad (2.4)$$

where the kernel is still given by Eq. (2.2), assuming that the spatial dependence of the long-range interaction does not change because of the flow.

To perform analytical calculations using Eq. (2.4), we obtain its dimensionless version using the following scaled quantities,

$$\mathbf{x} \rightarrow R\mathbf{u}; \quad t \rightarrow \frac{\tau R^2}{D}; \quad \rho(\mathbf{x}, t) \rightarrow \frac{D}{R^2\beta}\tilde{\rho}(\mathbf{u}, \tau); \quad G(\mathbf{x}) \rightarrow \frac{H(\mathbf{u})}{R^2}, \quad (2.5)$$

Note that the scaled kernel remains normalized, $\int_E H(\mathbf{u})d\mathbf{u} = 1$. Using these scaled variables, we get

$$\frac{\partial \rho(\mathbf{u}, \tau)}{\partial \tau} = \text{Da}\rho(\mathbf{u}, \tau) + \nabla_{\mathbf{u}}^2\rho(\mathbf{u}, \tau) - \rho(\mathbf{u}, \tau) \int_E H(\mathbf{u} - \mathbf{v})\rho(\mathbf{v}, \tau)d\mathbf{v} - \overline{\text{Pe}}\mathbf{f}(\mathbf{u}) \cdot \nabla_{\mathbf{u}}\rho(\mathbf{u}, \tau) \quad (2.6)$$

where E is the scaled domain, with lateral length L/R and still with periodic boundary conditions, and we have omitted the tildes from the density field. We have, moreover, defined two dimensionless control parameters

$$\text{Da} = \frac{rR^2}{D} \quad \text{and} \quad \overline{\text{Pe}} = \frac{v_0R}{D} \quad (2.7)$$

that are, respectively, the diffusive Damköhler number and a characteristic Péclet number. Finally, in the spatial structure of the velocity field, we have simply replaced $\mathbf{f}(\mathbf{x}) \rightarrow \mathbf{f}(\mathbf{u})$ because it is already dimensionless.

2.2 Flow models

We consider two stationary two-dimensional flows in a system of size $L \times L$ and periodic boundary conditions. This choice of environmental flows allows us to investigate how different spatial forms of fluid strain distort the emergent pattern of population density and how these changes in the pattern impact the long-term population size. The two flows we consider are:

Sine flow. We first consider a sine flow where only the horizontal velocity is non-zero, and its

intensity changes with the vertical coordinate. Already using scaled variables and absorbing the typical velocity scale in $\overline{\text{Pe}}$, the velocity field is defined by a vectorial function $\mathbf{f}(\mathbf{u})$ with components

$$f_u(u, v) = \sin(m\tilde{q}v), \quad (2.8)$$

$$f_v(u, v) = 0, \quad (2.9)$$

where $\tilde{q} = 2\pi R/L$ is the fundamental frequency of the sine flow and m is a positive integer number that sets the number of flow periods in the system (see Panel A of Fig. A1 for the vector field generated by this flow). We used $m = 1$ in all the analyses. For this simple shear flow, the shear rate (proportional to the derivative of f_u with respect to v) oscillates in the v coordinate in anti-phase with the velocity.

Rankine vortex flow. Second, we use a Rankine velocity field with radial symmetry [53], which we modify to make it suitable for the use of periodic boundary conditions [33, 54]. The Rankine vortex is a classic example of an irrotational vortex flow that corrects the singularity of the velocity at the vortex center by assuming that, in this region, the motion of the flow resembles the rotation of a solid body. In polar coordinates, the radial component of the velocity v_r is zero, and the angular component depends on the distance to the center of the vortex as

$$v_\theta(r, \theta) = \begin{cases} \frac{\Gamma r}{a} & \text{if } 0 \leq r < a, \\ \frac{\Gamma a}{r} & \text{if } r \geq a \end{cases} \quad (2.10)$$

where r is the radial distance to the center of the vortex, which we placed at the center of the simulation domain; a is the distance at which the intensity of flow reaches its maximum; and Γ is the maximum vortex circulation. This parameter also defines the vortex spinning direction: counterclockwise for positive Γ and clockwise for Γ negative.

Because the vortex velocity field defined by Eq. (2.10) has an infinite range, considering periodic boundary conditions leads to a velocity field involving two infinite sums (see [54] for a detailed derivation using the point vortex model, which is also valid for the Rankine vortex if $a \ll L$). We can reduce the velocity field created by a periodic array of vortices to an expression in cartesian

coordinates that only uses one summation [33, 54, 55]

$$v_x(\Delta x, \Delta y) = -\frac{\Gamma}{2L} \sum_{m=-\infty}^{\infty} \frac{\sin\left(\frac{2\pi\Delta y}{L}\right)}{\cosh\left[2\pi\left(\frac{\Delta x}{L} + m\right)\right] - \cos\left(\frac{2\pi\Delta y}{L}\right)}, \quad (2.11)$$

$$v_y(\Delta x, \Delta y) = \frac{\Gamma}{2L} \sum_{m=-\infty}^{\infty} \frac{\sin\left(\frac{2\pi\Delta x}{L}\right)}{\cosh\left[2\pi\left(\frac{\Delta y}{L} + m\right)\right] - \cos\left(\frac{2\pi\Delta x}{L}\right)}, \quad (2.12)$$

where $\Delta x = x - L/2$ and $\Delta y = y - L/2$. We can truncate Eqs. (2.11) and (2.12) at the first terms in m because the intensity of the velocity field decays proportionally to r^{-1} and thus only vortices in the closest neighbors of the focal cell contribute to the velocity flow within it. Finally, we can define the characteristic velocity of this vortex flow $v_0 = \Gamma/2L$, which allows us to define the characteristic Péclet number $\overline{\text{Pe}}$. In all the simulations we performed using this periodic Rankine vortex flow, we used $a = 0.05L$.

3 Results

3.1 Pattern formation in the nonlocal spatial logistic model without flow

We first study the case without environmental flow $\mathbf{f}(\mathbf{u}) = 0$ to use it as a baseline to quantify the effect of advection both on the spatial patterns of population density and the long-term population size. We study this no-flow limit analytically via a linear stability analysis of Eq. (2.1) and perform numerical simulations of the fully nonlinear equation (see App. A for details of the pseudospectral methods we used and [GitHub](#) for the code repository). The linear stability analysis is a standard technique in pattern-formation theory that consists on adding small spatial perturbations to one of the uniform solutions of the fully nonlinear model and obtaining the short-term linearized perturbation growth rate [56]. If this perturbation growth rate is positive for a certain wavenumber, then perturbations with that periodicity will grow over time, and the system may exhibit spatial patterns. Otherwise, the perturbation decays, meaning that the uniform solution is stable against small spatial perturbations.

To perform this linear stability analysis we first consider the scaled nonlocal logistic model in Eq. (2.6) with the velocity field set to zero and consider a perturbed solution of the form $\rho(\mathbf{u}, \tau) = \rho_0 + \epsilon\psi(\mathbf{u}, \tau)$ where $\rho_0 = \text{Da}$ is the equilibrium uniform solution, and $\epsilon \ll 1$. The linearized dynamics of the perturbation is given by

$$\frac{\partial\psi(\mathbf{u}, \tau)}{\partial\tau} = \nabla_{\mathbf{u}}^2\psi(\mathbf{u}, \tau) - \text{Da} \int_E H(\mathbf{u} - \mathbf{v})\psi(\mathbf{v}, \tau)d\mathbf{v}, \quad (3.1)$$

which is a linear equation that we can solve using the Fourier transform. Fourier transforming Eq. (3.1) and considering that $\hat{\psi}(\mathbf{k}, t) \propto \exp(-\lambda(\mathbf{k})t)$ because the transformed equation is linear, we obtain an equation for the perturbation growth rate

$$\lambda(k) = -k^2 - \text{Da} \hat{H}(k) \quad (3.2)$$

where $\hat{H}(k)$ is the Fourier transform of the scaled competition kernel, and $k = |\mathbf{k}|$ is the modulus of the wavevector \mathbf{k} (which is already scaled by R as it is \mathbf{u}). Because the first term on the right side of Eq. (3.2) is always negative and Da is a positive constant, pattern formation requires that the Fourier transform of the competition kernel must be negative for some wavenumber k [43–45]. The Fourier transform of the scaled top-hat kernel, $H(\mathbf{u})$ we introduced in Eq. (2.5) is

$$\hat{H}(k) = 2 \frac{J_1(k)}{k}, \quad (3.3)$$

where J_1 is the order-1 Bessel function of the first kind and thus an oscillatory function taking negative values for some wavevector modulus k . Therefore, when Da is large enough, $\text{Da} > \text{Da}_c \approx 185.192$, the uniform distribution of population density becomes unstable and patterns form. In the numerical simulations of the fully nonlinear equation, we observe that these patterns have a hexagonal symmetry. This spatial configuration minimizes competition throughout the entire system and hence leads to higher population abundances than in the uniform case (Fig. 1).

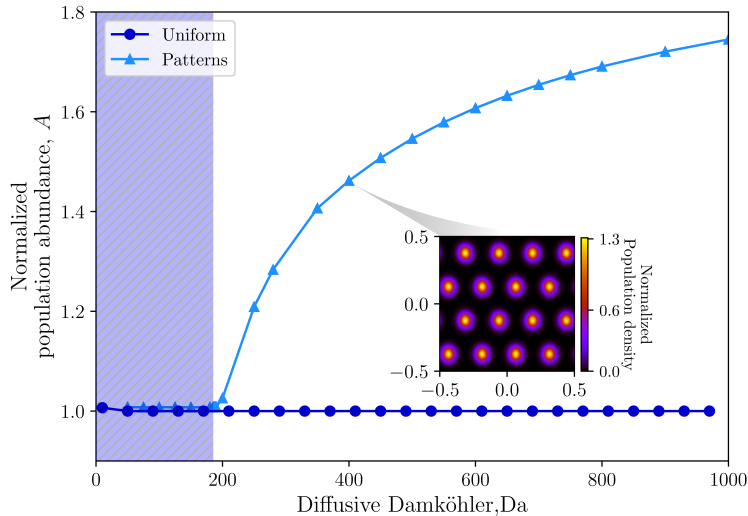


Figure 1: Normalized long-term population abundance as a function of Da for the patterned and uniform distributions of population density in the absence of flow. The blue-shaded region highlights the non-pattern parameter regime where $\text{Da} < \text{Da}_c \approx 185.192$. The inset shows a typical pattern for $\text{Da} > \text{Da}_c$.

3.2 Effect of environmental flows

Next, we study how advection by the flows introduced in Section 2.2 modifies the patterns forming due to long-range competition and how these new spatial configurations of the population density impact the dynamics and the total population size. We perform these analyses by combining numerical simulations of Eq. (2.6) and, when possible, analytical approximations.

3.2.1 Sine flow

To get a first understanding of how the sine flow might impact pattern formation in our model, we extend the linear stability analysis of Section 3.1 to account for an advection term with a velocity field given by Eqs. (2.8)-(2.9) with $m = 1$ (see App. B for the details of the calculation). The linearized dynamics of a perturbation to the uniform solution is now given by

$$\frac{\partial \psi(\mathbf{u}, \tau)}{\partial \tau} = \nabla_{\mathbf{u}}^2 \psi(\mathbf{u}, \tau) - \text{Da} \int_E H(\mathbf{u} - \mathbf{v}) \psi(\mathbf{v}, \tau) d\mathbf{v} - \overline{\text{Pe}} \sin(\tilde{q}v) \frac{\partial \psi(\mathbf{u}, \tau)}{\partial u}. \quad (3.4)$$

Because the system is periodic, we can use a Floquet decomposition of the perturbation that gives a general expression for the perturbation growth rate

$$\left[\lambda(\mathbf{k}) + k_n^2 + \nu \hat{H}(\mathbf{k}_n) \right] C_n(\mathbf{k}) = k_u \frac{\overline{\text{Pe}}}{2} [C_{n+1}(\mathbf{k}) - C_{n-1}(\mathbf{k})] \quad n = 0, 1, 2, \dots \quad (3.5)$$

where $C_n(\mathbf{k})$ are Fourier-Floquet coefficients of the perturbation and we have defined $\mathbf{k}_n = (k_u, k_v + n\tilde{q})$ for $n = 0, 1, 2, \dots$ (see App. B). Note also that, for $\overline{\text{Pe}} = 0$ or $k_u = 0$, Eq. (3.5) reduces to the expression for the perturbation growth rate we derived without flow, Eq. (3.2). Thus, the value of $\lambda(k_u = 0, k_v)$ is not affected by the flow, and the instability at $k_u = 0$ leading to horizontal stripes will appear at the same value of Da_c as in the absence of flow. We have to investigate if other types of instabilities appear at lower values of Da or if this is the first instability of the homogeneous solution encountered when increasing Da . To this end, in the $\overline{\text{Pe}} \ll 1$ limit, we can truncate the system of equations in Eq. (3.5) to only consider $n = 0, \pm 1$. This type of system has a non-trivial solution only if the determinant of the coefficient matrix is zero, which gives us three eigenvalues $\lambda_0(\mathbf{k})$, and $\lambda_{\pm}(\mathbf{k})$. By numerically analyzing the behavior of these eigenvalues, we find that the real part of the largest eigenvalue becomes positive at the same value $\text{Da} = \text{Da}_c$ as in the absence of flow, indicating that the sine flow does not play any role in setting the onset of pattern formation (Fig. A2).

Numerical simulations of the full, nonlinear equation confirm the theoretical prediction that the sine flow does not change the value of the Damköhler number at which the uniform solution loses stability and patterns form (Fig. 2A, Fig. A3). Increasing Da at any fixed value of $\overline{\text{Pe}}$, the

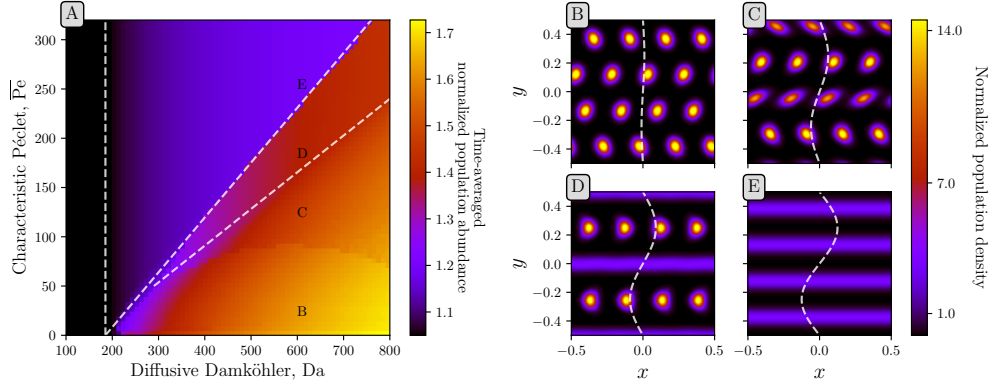


Figure 2: A) Long-term total population abundance averaged after time as a function of Damköhler number and the maximum \overline{Pe} . We performed the time average at $t > 2000$, sampling the spatial configuration until the relative standard error of this temporal average was below 1%. The white dashed lines limit the regions with the different spatial patterns shown in (B-E), and they are computed using the derivative of the average total population size (Fig. A3). B-E) Snapshots of the spatial pattern once the system reaches an asymptotic state. We find four possible spatiotemporal patterns with increasing flow intensity: (B) spots moving horizontally ($Da = 600, \overline{Pe} = 20$), (C) stretched moving spots ($Da = 600, \overline{Pe} = 120$), (D) coexisting spots and stripes ($Da = 600, \overline{Pe} = 180$), and (E) stripes ($Da = 600, \overline{Pe} = 250$) (see [SM Videos](#) for the pattern formation dynamics)

first instability appearing on the homogeneous state leads to horizontal stripes, in agreement with the linear stability analysis sketched above and in Appendix B. Moreover, the spot-stripe pattern transition only depends on the ratio \overline{Pe}/Da and is thus independent of the specific value of the diffusion constant provided that D is low enough to allow for pattern formation in the absence of advection.

When we explore the full (Da, \overline{Pe}) parameter space, however, we find that the environmental flow leads to a very rich diversity of outcomes, both in terms of the spatial patterns and the total population size. As expected from the analysis without flow, the population abundance increases with the Damköhler number Da . Increasing the maximum flow intensity \overline{Pe} , however, reduces the total population abundance because the flow deforms the hexagonal pattern of circular spots (inset of Figs. 1 and 2) and makes neighbor spots compete with each other.

The changes in total population size are not smooth over the entire parameter space, as can be observed by computing the modulus of the gradient of the total population size with respect to \overline{Pe} and Da (Fig. A3). Non-smooth changes in the total population size as the Damköhler and Péclet numbers vary allow us to define at least three different regions within the parameter space (assuming $Da > Da_c$; see Fig. A3). In the first region, in the bottom right corner of Fig. 2A, the flow stretches and transports the population clumps horizontally, making the pattern non-stationary and formed by elliptic spots (Figs. 2B, C and [SM Video 1](#), [SM Video 2](#)). Within this region, we observe a discontinuity in the derivative of total population abundance at a Da -specific value of

the characteristic Péclet number (see the concave down curve in lighter purple of Fig. A3). Higher values of $\overline{\text{Pe}}$ increase the stretch of the spots, which makes spots in the same pattern row interact more strongly with their neighbors. We think that this increased competition between neighbor spots could cause this non-smooth decay in the time-averaged population density, but were not able to quantify this phenomenon in the simulations. As $\overline{\text{Pe}}$, and consequently shear, continues to increase, spots placed in the high-shear regions of the environment are fully stretched and become stripes (Fig. 2D; SM Video 3). Finally, when the ratio between $\overline{\text{Pe}}$ and Da is high, the shear of the flow is strong enough to break the spots everywhere in the environment, and stripes aligned with the flow velocity form everywhere in the system (Fig. 2E; SM Video 4).

To have a more quantitative understanding of how patterns change with increasing shear rate, we measure how increasing $\overline{\text{Pe}}$ stretches the population clusters. To measure this cluster stretching, we use the Taylor deformation parameter, defined as

$$\Delta = \frac{d_1 - d_2}{d_1 + d_2}, \quad (3.6)$$

where d_1 and d_2 are the semi-major and semi-minor axis of the stretched spot. In the absence of flows, spots are approximately circular, so $d_1 \approx d_2$ and $\Delta \approx 0$ ($d_1 = d_2$ only for very fine space discretization). To obtain the values of d_1 and d_2 , we first binarized the pattern image using a threshold method. In this binarized image, we computed the major axis of the pattern spot d_1 by numerically searching the pair of points at the spot boundary with the largest distance between them. Finally, we computed the minor axis d_2 as the orthogonal line to d_1 . The Taylor deformation parameter increases linearly with $\overline{\text{Pe}}$ (Fig. 3), and therefore, the effect of the shear rate on the pattern shape is proportional to the intensity of the shear itself. Notice that we only measure Δ for patterns in the regions B and C of Fig. 2 because the Taylor deformation parameter is not defined for stripes.

Next, we looked at how the changes in the spatial pattern induced by the shear (transport and stretch of the population density spots) impact the time series of population abundance (Fig. 4). For low $\overline{\text{Pe}}$ (B and C regions), the total population abundance oscillates, and the frequency of these oscillations is determined by the wavelength of the pattern and the speed at which the environmental flow changes the symmetry of the pattern as it transports its spots. Without the flow, the spots have a hexagonal symmetry typical of competition-induced patterns that maximizes population size because it minimizes competition [11, 44]. A weak sine flow, however, transports rows of clusters in the x direction, making them periodically interact with the spots in the upper and lower rows and inducing oscillations in the total population size.

To characterize these oscillations quantitatively, we computed the power spectrum of the time

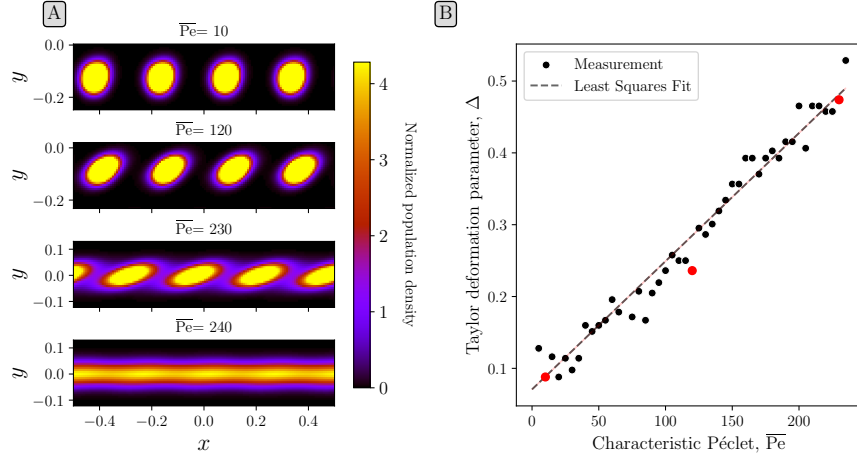


Figure 3: A) Shape of the population clumps that form in the regions of the simulation domain with high shear for $Da = 800$. Notice the difference in the range of the y -axis from top to bottom because the full spatial pattern arranges differently in the simulation domain for different values of \overline{Pe} . B) Taylor deformation parameter Δ as a function of \overline{Pe} for $Da = 800$. The deformation is measured for the population clumps forming in the pattern region with higher shear. The dots correspond to the values measured directly from the simulated patterns and the dashed line is a linear regression fit using the method of least squares. Dots highlighted in red correspond to the same \overline{Pe} values for which the spatial pattern is shown in panel A.

series of total population abundance, which we obtained as the integral of the spatial pattern over the system size. These power spectra show a peaked maximum at a non-zero frequency that corresponds with the natural frequency at which population size oscillates (Fig. 4B). To test whether the total population size oscillates due to the transport of the spots by the environmental flow as described previously, we calculate the frequency at which the pattern goes from a hexagonal to a square structure as rows of spots are transported, at a y -dependent velocity, by the flow. We can obtain this frequency by approximating spots by a point particle placed at the spot center and calculating the time this punctual particle needs to travel a distance equal to one-half of the pattern wavelength. When the flow is weak so that spots are not stretched, the results obtained from this mapping return an excellent agreement with the frequency extracted from the power spectra of the simulations, ω_{\max} (Fig. 4C). At higher \overline{Pe} , however, the flow stretches the spots and the pattern loses the hexagonal structure, which makes this approximation fail.

3.2.2 Rankine vortex flow

The results obtained with a sine flow suggest that the interplay between the spatial structure of the flow velocity field and the spatial pattern is key to determining population dynamics. To explore this connection deeper, we next investigate a scenario with a Rankine vortex flow which has a radial symmetry that is not aligned with any of the primitive vectors of the hexagonal pattern that forms

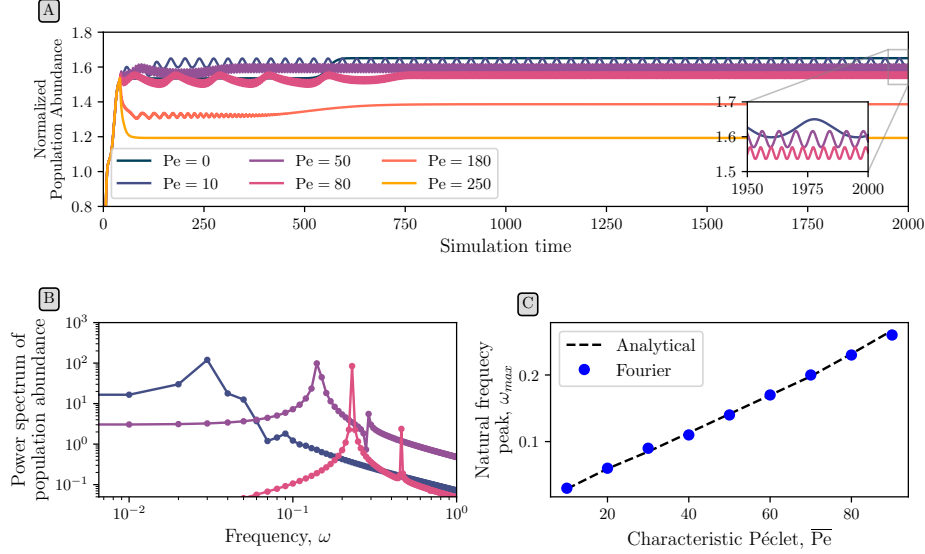


Figure 4: A) Time series of the normalized population abundance for the sine flow, $Da = 600$, and different values of \overline{Pe} . B) Log-log power spectrum of the time series of total population size in the long-time limit (between $t \in [800, 2000]$). C) Natural frequency of the total population time-series, defined as the frequency at which the power spectrum reaches its maximum value, as a function of \overline{Pe} . Blue dots correspond to the values extracted from the power spectra obtained from numerical simulations and the black dashed line shows the values obtained by approximation population-density clumps by point-like particles centered at the clump center.

without advection. For this flow, the linear stability analysis of the uniform solution becomes too difficult and, thus, we describe in the following the results of numerical simulations.

For this Rankine flow, the time-averaged total population size also decreases with increasing \overline{Pe} and, as expected, increases with the Damköhler number Da (Fig. 5). The emergent spatiotemporal patterns of population density are, however, much more complex than those produced by the sine flow. First, we observe that the rotational velocity shifts the transition to patterns to higher values of the Damköhler number (Figs. 5). Moreover, the shift in Da_c increases when \overline{Pe} until it plateaus for sufficiently large Péclet. Regarding the pattern dynamics, the circular movement of clusters caused by the radial symmetry of the velocity field makes them interact more with each other, including the possibility of spot-splitting annihilation dynamics that we did not observe for the sine flow.

Because the spots of population density undergo this more complex spatiotemporal dynamics, we cannot divide the parameter space into well-defined regions using a quantitative criterium as we did for the sine flow (see Fig. A4). Instead, we systematically explore the parameter space and describe the different types of spatiotemporal patterns we observe. For low Da and low \overline{Pe} , the pattern rotates around the central spot that resides inside the region where the angular velocity increases linearly with r (Fig. 5B and SM Video 5). When Da is still low, but \overline{Pe} increases, the vortex origin

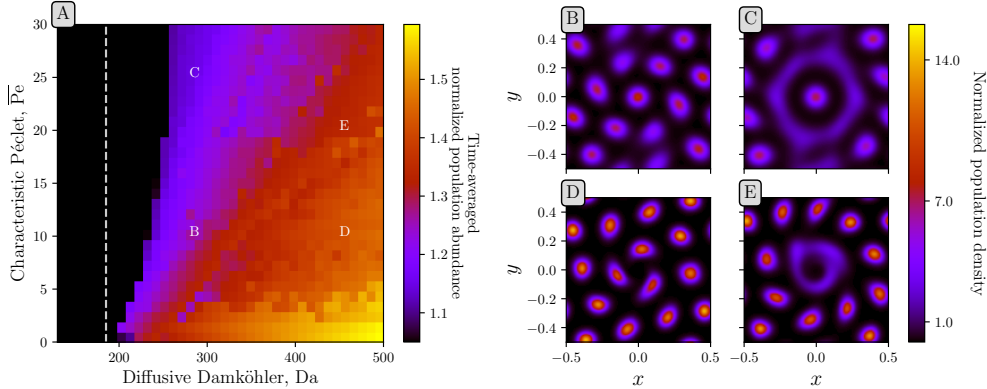


Figure 5: A) Long-term normalized population abundance averaged over time, computed following the same steps used in Fig. 2, as a function of the Damköhler and Péclet numbers, Da and \overline{Pe} , respectively. The white dashed line marks the value of the Damköhler number Da_c at which patterns form without flow. B-E) Snapshots of the long-term spatial pattern: (B) rotating spots ($Da = 280$, $\overline{Pe} = 10$); (C) central spot surround by a ring of creation-annihilation spots ($Da = 280$, $\overline{Pe} = 25$); (D) stretched rotating spots ($Da = 450$, $\overline{Pe} = 10$); and (E) central ring surrounded by rotating spots ($Da = 200$, $\overline{Pe} = 25$) (see SM Videos 5-8 for the pattern formation dynamics)

is populated and surrounded by a ring of population density where spots are constantly absorbed and ejected (Fig. 5C; SM Video 6). At larger values of Da , the central region of the environment is occupied by three stretched spots that rotate in a direction given by the vortex circulation (Fig. 5D; SM Video 7). Within this high- Da regime, the pattern keeps the same qualitative organization we found in Fig. 5D when \overline{Pe} increases. However, due to higher stretching in the spots, the gap between the stretched spots closes and these form a stable ring (Fig. 5E; SM Video 8)

Finally, we investigated the consequences of this more complex spatiotemporal dynamics on the time series of the total population size. The rich variety of possible spatiotemporal patterns makes it hard to classify systematically all the possible dynamics exhibited by the total population size. Instead, we discuss a few examples to illustrate the richness of behaviors that emerge when the velocity field is not aligned with one of the primitive vectors of the population density pattern (triangular lattice). For regions of the parameter space where spots split and merge, the temporal dynamics of the total population is erratic, with large changes corresponding to the formation (and growth) or annihilation of spots (Fig. 6A). This erratic time series fluctuates in time without a characteristic frequency (Fig. 6B). When \overline{Pe} increases, the central ring becomes a stable structure in which aggregates of population density do not split and merge. As a result, the population abundance oscillates in time with a characteristic oscillation frequency, similar to what we observed for the sine flow (lighter curves in Fig. 6).

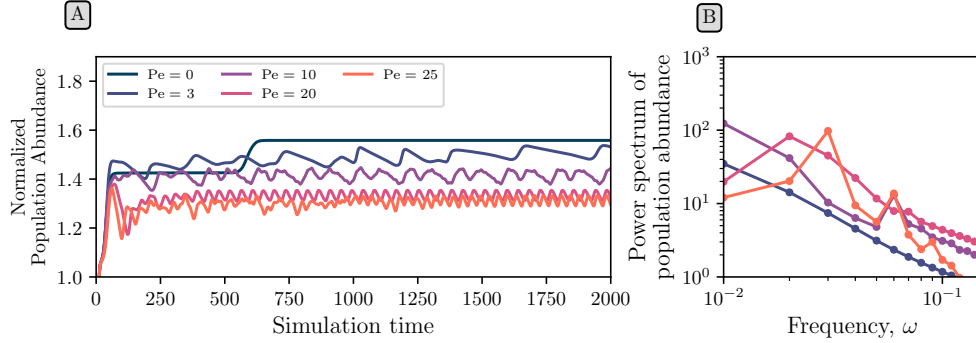


Figure 6: A) Time series of the normalized population abundance for the Rankine vortex flow and $Da = 450$ and different values of \overline{Pe} . B) Log-log power spectrum of the time series in panel A in the long-time limit ($t \in [1000, 2000]$).

4 Discussion

We extended the nonlocal logistic model to theoretically investigate how transport and shear in a flow environment reshape spatial patterns of population density and how these pattern changes are reflected in the dynamics of the population abundance. The flow changes the spatiotemporal properties of the emergent patterns of population density and, for certain flow structures, delays the onset of pattern formation to higher values of the nonlocal spatial coupling (or in other words, flows tend to stabilize uniform distributions of population density). Weak flows make patterns non-stationary by transporting and stretching density spots, which leads to different types of oscillations in the population abundance depending on the relationship between the spatial structures of the pattern and the flow. Stronger flows stretch population aggregates enough to merge them with their closest neighbors, which leads to a stationary pattern in which the population abundance does not oscillate and whose shape follows the flow streamlines. This is what we find for the two flows studied when increasing Da at constant large \overline{Pe} .

An explicit description of the environmental conditions and biophysical processes taking place as patterns form is thus important not only to characterize pattern formation *per se*, but also to better understand its ecological consequences. Here, we considered a single-species model where organisms interact with each other only via intraspecific competition. For this particular choice of ecological dynamics, patterns form to minimize competition and thus adopt a hexagonal symmetry in two-dimensional environments. Because the flow perturbs this configuration by making population clusters interact with each other, flow environments always exhibit smaller population sizes than non-flow environments. In cases with more complex ecological dynamics, including communities with different interactions, flow-induced changes in the spatial patterns of population density may shift the equilibrium state in different directions. Previous work has shown that spatial patterns

induced by nonlocal interactions can prevent competitive exclusion by segregating species in space [13, 57] or change the demographic properties of Allee effects [11]. Our results suggest that these pattern-induced phenomena could be very sensitive to the presence of flows. Flows could, for example, prevent competing species from segregating in space, as shown in [13, 57], forcing them to interact periodically and ultimately causing the extinction of the weaker competitor.

Besides choosing a simple ecological scenario, we simplified the mixing process by choosing incompressible and stationary flows. Non-stationary flows allow for a much richer variety of mixing processes, including chaotic regimes whose statistical properties mimic those of turbulent environments [58]. In these regimes, the flow can create regions of different mixing, including ones where organisms remain trapped for a longer time and interact more often with their neighbors [26, 59]. This flow-induced heterogeneity in species interactions can impact ecological processes, such as plankton blooms [60] and pathogen transmission [61], and alter the outcome of evolutionary dynamics [54, 62]. Transport properties also change when considering compressible flows, which impacts population mixing [63, 64]. Previous work in local models of population dynamics has shown that considering mixing by compressible flows can importantly impact both the spatial distribution of organisms and the long-term ecological and evolutionary dynamics [31, 35, 65, 66]. Therefore, investigating the emergent spatial patterns and population dynamics due to nonlocal interactions in environments with compressible or chaotic flows is an interesting direction for future research.

Acknowledgments

This work was partially funded by the Center of Advanced Systems Understanding (CASUS), which is financed by Germany's Federal Ministry of Education and Research (BMBF) and by the Saxon Ministry for Science, Culture and Tourism (SMWK) with tax funds on the basis of the budget approved by the Saxon State Parliament. NS was partially supported by Coordenação de Aperfeiçoamento de Pessoal de Nível Superior (CAPES) - Finance Code 001 and by the CAPES-Print program through a sandwich doctoral fellowship at CASUS, Germany. RMG and JV were partially supported by FAPESP through a BIOTA Jovem Pesquisador Grant 2019/05523-8 (RMG and JV), ICTP-SAIFR grant 2021/14335-0 (RMG), and a Master's fellowship 2020/14169-0 (JV). RMG acknowledges support from Instituto Serrapilheira (Serra-1911-31200). C.L. and E.H-G were supported by grants LAMARCA PID2021-123352OB-C32 funded by MCIN/AEI/10.13039/501100011033323 and FEDER "Una manera de hacer Europa"; and TED2021-131836B-I00 funded by MICIU/AEI/10.13039/501100011033 and by the European Union "NextGenerationEU/PRTR". E.H-G. also acknowledges the Maria de Maeztu program for Units of Excellence, CEX2021-001164-M funded by MCIN/AEI/10.13039/501100011033. C.L was partially supported by the Scultetus Center Visiting

References

- [1] Martinez-Garcia R, Tarnita CE, Bonachela JA. Self-organized patterns in ecological systems: from microbial colonies to landscapes. *Emerging Topics in Life Sciences*. 2022;6(3):245-58. doi:10.1042/ETLS20210282.
- [2] Pringle RM, Tarnita CE. Spatial Self-Organization of Ecosystems: Integrating Multiple Mechanisms of Regular-Pattern Formation. *Annual Review of Entomology*. 2017 jan;62(1):359-77. doi:10.1146/annurev-ento-031616-035413.
- [3] Karig D, Martini KM, Lu T, DeLateur NA, Goldenfeld N, Weiss R. Stochastic Turing patterns in a synthetic bacterial population. *Proceedings of the National Academy of Sciences*. 2018;115(26):6572-7.
- [4] Rietkerk M, Bastiaansen R, Banerjee S, van de Koppel J, Baudena M, Doelman A. Evasion of tipping in complex systems through spatial pattern formation. *Science*. 2021;374(6564):eabj0359. doi:10.1126/science.abj0359.
- [5] Martinez-Garcia R, Cabal C, Calabrese JM, Hernández-García E, Tarnita CE, López C, et al. Integrating theory and experiments to link local mechanisms and ecosystem-level consequences of vegetation patterns in drylands. *Chaos, Solitons & Fractals*. 2023;166:112881.
- [6] Rietkerk M, van de Koppel J. Regular pattern formation in real ecosystems. *Trends in ecology & evolution*. 2008;23(3):169–175.
- [7] Zhong Y, Bracco A, Villareal TA. Pattern formation at the ocean surface: Sargassum distribution and the role of the eddy field. *Limnology and Oceanography: Fluids and Environments*. 2012;2(1):12-27.
- [8] Ruiz-Reynés D, Gomila D, Sintes T, Hernández-García E, Marbà N, Duarte CM. Fairy circle landscapes under the sea. *Science Advances*. 2017;3(8):e1603262.
- [9] Sun J, Li X, Chen N, Wang Y, Song G. Regular pattern formation regulates population dynamics: Logistic growth in cellular automata. *Ecological Modelling*. 2020 February;418:108878. doi:10.1016/j.ecolmodel.2019.108878.
- [10] Surendran A, Plank MJ, Simpson MJ. Population dynamics with spatial structure and an Allee effect. *Proceedings of the Royal Society A: Mathematical, Physical and Engineering Sciences*. 2020;476:1–19.

- [11] Jorge DCP, Martinez-Garcia R. Demographic effects of aggregation in the presence of a component Allee effect. *Journal Royal Society Interface*. 2024 June;21:20240042. doi:10.1101/2023.05.12.540532.
- [12] de Roos AM, McCauley E, Wilson WG. Pattern formation and the spatial scale of interaction between predators and their prey. *Theoretical population biology*. 1998;53(2):108-30.
- [13] Maciel GA, Martinez-Garcia R. Enhanced species coexistence in Lotka-Volterra competition models due to nonlocal interactions. *Journal of Theoretical Biology*. 2021;530:110872. doi:10.1016/j.jtbi.2021.110872.
- [14] Eigentler L. Species coexistence in resource-limited patterned ecosystems is facilitated by the interplay of spatial self-organisation and intraspecific competition. *Oikos*. 2021;130:609-23.
- [15] Martinez-Calvo A, Wingreen NS, Datta SS. Pattern formation by bacteria-phage interactions. *bioRxiv*. 2023:2023-09.
- [16] Wakano JY, Nowak MA, Hauert C. Spatial dynamics of ecological public goods. *Proceedings of the National Academy of Sciences of the United States of America*. 2009;106(19):7910-4. doi:10.1073/pnas.0812644106.
- [17] Park HJ, Gokhale CS. Ecological feedback on diffusion dynamics. *Royal Society open science*. 2019;6(2):181273.
- [18] Mimura M. Stationary pattern of some density-dependent diffusion system with competitive dynamics. *Hiroshima Mathematical Journal*. 1981;11(3):621-35.
- [19] Martinez-Garcia R, Murgui C, Hernández-García E, López C. Pattern Formation in Populations with Density-Dependent Movement and Two Interaction Scales. *PLoS ONE*. 2015;10:e0132261. doi:10.1371/journal.pone.0132261.
- [20] Liu QX, Herman PMJ, Mooij WM, Huisman J, Scheffer M, Olf H, et al. Pattern formation at multiple spatial scales drives the resilience of mussel bed ecosystems. *Nature Communications*. 2014;5:1-7. doi:10.1038/ncomms6234.
- [21] Liu QX, Rietkerk M, Herman PM, Piersma T, Fryxell JM, van de Koppel J. Phase separation driven by density-dependent movement: a novel mechanism for ecological patterns. *Physics of life reviews*. 2016;19:107-21.
- [22] Farrell F, Marchetti M, Marenduzzo D, Tailleur J. Pattern formation in self-propelled particles with density-dependent motility. *Physical review letters*. 2012;108(24):248101.

- [23] Cates ME, Tailleur J. Motility-induced phase separation. *Annu Rev Condens Matter Phys.* 2015;6(1):219-44.
- [24] Young WR, Roberts AJ, Stuhne G. Reproductive pair correlations and the clustering of organisms. *Nature.* 2001 July;412(6844):328-31. doi:10.1038/35085561.
- [25] Guasto JS, Rusconi R, Stocker R. Fluid mechanics of planktonic microorganisms. *Annual Review of Fluid Mechanics.* 2012;44(1):373-400.
- [26] Neufeld Z, Hernández-García E. Chemical and biological processes in fluid flows: a dynamical systems approach. World Scientific; 2009.
- [27] Visser AW, Kiørboe T. Plankton motility patterns and encounter rates. *Oecologia.* 2006;148:538-46.
- [28] Ser-Giacomi E, Martinez-Garcia R, Dutkiewicz S, Follows MJ. A Lagrangian model for drifting ecosystems reveals heterogeneity-driven enhancement of marine plankton blooms. *Nature Communications.* 2023;14:6092. doi:10.1038/s41467-023-41469-2.
- [29] Comesaña A, Fernández-Castro B, Chouciño P, Fernández E, Fuentes-Lema A, Gilcoto M, et al. Mixing and phytoplankton growth in an upwelling system. *Frontiers in Marine Science.* 2021;8:712342.
- [30] Martin A. Phytoplankton patchiness: the role of lateral stirring and mixing. *Progress in oceanography.* 2003;57(2):125-74.
- [31] Pigolotti S, Benzi R, Jensen MH, Nelson DR. Population Genetics in Compressible Flows. *Physical Review Letters.* 2012 March;108(12):128102. doi:10.1103/PhysRevLett.108.128102.
- [32] Uppal G, Vural DC. Shearing in flow environment promotes evolution of social behavior in microbial populations. *eLife.* 2018;7:e34862.
- [33] Krieger MS, Sinai S, Ferrari R, Nowak MA, Aug PE. Turbulent coherent structures and early life below the Kolmogorov scale. *Nature Communications.* 2020;11:2192.
- [34] Benzi R, Nelson DR, Shankar S, Toschi F, Zhu X. Spatial population genetics with fluid flow. *Reports on Progress in Physics.* 2022 August;85(9):096601. Publisher: IOP Publishing. doi:10.1088/1361-6633/ac8231.
- [35] Plummer A, Benzi R, Nelson DR, Toschi F. Fixation probabilities in weakly compressible fluid flows. *Proceedings of the National Academy of Sciences of the United States of America.* 2019;116(2):373-8. doi:10.1073/pnas.1812829116.

- [36] van de Vijssel RC, Hernández-García E, Orfila A, Gomila D. Optimal wave reflection as a mechanism for seagrass self-organization. *Scientific Reports*. 2023;13(1):20278.
- [37] Vasquez DA, Meyer J, Suedhoff H. Chemical pattern formation induced by a shear flow in a two-layer model. *Phys Rev E*. 2008 Sep;78:036109. doi:10.1103/PhysRevE.78.036109.
- [38] Stucchi L, Vasquez DA. Pattern formation induced by a differential shear flow. *Phys Rev E*. 2013 Feb;87:024902. doi:10.1103/PhysRevE.87.024902.
- [39] Fuentes MA, Kuperman MN, Kenkre VM. Nonlocal interaction effects on pattern formation in population dynamics. *Physical Review Letters*. 2003;91(15):3-6. doi:10.1103/PhysRevLett.91.158104.
- [40] Berestycki H, Nadin G, Perthame B, Ryzhik L. The non-local Fisher–KPP equation: travelling waves and steady states. *Nonlinearity*. 2009 October;22(12):2813. doi:10.1088/0951-7715/22/12/002.
- [41] Scheffer M, van Nes EH. Self-organized similarity, the evolutionary emergence of groups of similar species. *Proceedings of the National Academy of Sciences of the United States of America*. 2006 apr;103(16):6230-5. doi:10.1073/pnas.0508024103.
- [42] Maruvka YE, Shnerb NM. Nonlocal competition and logistic growth: Patterns, defects, and fronts. *Physical Review E - Statistical, Nonlinear, and Soft Matter Physics*. 2006;73(1):1-12. doi:10.1103/PhysRevE.73.011903.
- [43] Pigolotti S, López C, Hernández-García E. Species Clustering in Competitive Lotka-Volterra Models. *Physical Review Letters*. 2007 jun;98(25):258101.
- [44] Hernández-García E, López C. Clustering, advection, and patterns in a model of population dynamics with neighborhood-dependent rates. *Physical review E, Statistical, nonlinear, and soft matter physics*. 2004 jan;70:016216.
- [45] López C, Hernández-García E. Fluctuations impact on a pattern-forming model of population dynamics with non-local interactions. *Physica D: Nonlinear Phenomena*. 2004;199(1):223-34. *Trends in Pattern Formation: Stability , Control and Fluctuations*. doi:<https://doi.org/10.1016/j.physd.2004.08.016>.
- [46] Martinez-Garcia R, Calabrese JM, Hernández-García E, López C. Vegetation pattern formation in semiarid systems without facilitative mechanisms. *Geophysical Research Letters*. 2013;40:6143-7.

- [47] Volpert V, Petrovskii S. Reaction–diffusion waves in biology. *Physics of Life Reviews*. 2009 December;6(4):267-310. doi:10.1016/j.plrev.2009.10.002.
- [48] Dornelas V, Colombo E, Anteneodo C. Single-species fragmentation: The role of density-dependent feedback. *Physical Review E*. 2019;99(6):062225.
- [49] da Silva L, Colombo E, Anteneodo C. Effect of environment fluctuations on pattern formation of single species. *Physical Review E*. 2014;90(1):012813.
- [50] Chandrasekhar S. Hydrodynamic and hydromagnetic stability. Courier Corporation; 2013.
- [51] Zahnw JC, Vilela RD, Feudel U, Tél T. Coagulation and fragmentation dynamics of inertial particles. *Physical Review E—Statistical, Nonlinear, and Soft Matter Physics*. 2009;80(2):026311.
- [52] Abel M, Cencini M, Vergni D, Vulpiani A. Front speed enhancement in cellular flows. *Chaos: An Interdisciplinary Journal of Nonlinear Science*. 2002 06;12(2):481-8. doi:10.1063/1.1457467.
- [53] Aref H. Integrable, chaotic, and turbulent vortex motion in two-dimensional flows. *Annual Review of Fluid Mechanics*. 1983;15(1):345-89.
- [54] Miranda JPV. The evolution of microbial cooperation under chaotic environmental flows [Master’s thesis]. São Paulo SP: Universidade Estadual Paulista (Unesp); 2023.
- [55] Weiss JB, McWilliams JC. Nonergodicity of point vortices. *Physics of Fluids A: Fluid Dynamics*. 1991 May;3(5):835-44. doi:10.1063/1.858014.
- [56] Cross MC, Hohenberg PC. Pattern formation outside of equilibrium. *Reviews of Modern Physics*. 1993;65(3).
- [57] Simoy MI, Kuperman MN. Non-local interaction effects in models of interacting populations. *Chaos, Solitons and Fractals*. 2023;167(November 2022). ArXiv: 2209.09761 Publisher: Elsevier Ltd. doi:10.1016/j.chaos.2022.112993.
- [58] Ottino JM, et al. Mixing, chaotic advection, and turbulence. *Annual Review of Fluid Mechanics*. 1990;22(1):207-54.
- [59] Zaslavsky G. Chaos, fractional kinetics, and anomalous transport. *Physics Reports*. 2002 December;371(6):461-580. doi:10.1016/S0370-1573(02)00331-9.
- [60] Reigada R, Hillary RM, Bees MA, Sancho JM, Sagués F. Plankton blooms induced by turbulent flows. *Proceedings of the Royal Society B: Biological Sciences*. 2003;270(1517):875-80. doi:10.1098/rspb.2002.2298.

- [61] Brookes JD, Antenucci J, Hipsey M, Burch MD, Ashbolt NJ, Ferguson C. Fate and transport of pathogens in lakes and reservoirs. *Environment International*. 2004;30(5):741-59.
- [62] Károlyi G, Neufeld Z, Scheuring I. Rock-scissors-paper game in a chaotic flow: The effect of dispersion on the cyclic competition of microorganisms. *Journal of Theoretical Biology*. 2005;236(1):12-20. doi:10.1016/j.jtbi.2005.02.012.
- [63] Vergassola M, Avellaneda M. Scalar transport in compressible flow. *Physica D: Nonlinear Phenomena*. 1997 July;106(1):148-66. doi:10.1016/S0167-2789(97)00022-5.
- [64] Volk R, Mauger C, Bourgoïn M, Cottin-Bizonne C, Ybert C, Raynal F. Chaotic mixing in effective compressible flows. *Physical Review E*. 2014 July;90(1):013027. Publisher: American Physical Society. doi:10.1103/PhysRevE.90.013027.
- [65] Perlekar P, Benzi R, Nelson DR, Toschi F. Population Dynamics At High Reynolds Number. *Physical Review Letters*. 2010 September;105(14):144501. Publisher: American Physical Society. doi:10.1103/PhysRevLett.105.144501.
- [66] Benzi R, Jensen MH, Nelson DR, Perlekar P, Pigolotti S, Toschi F. Population dynamics in compressible flows. *The European Physical Journal Special Topics*. 2012 April;204(1):57-73. doi:10.1140/epjst/e2012-01552-0.
- [67] Deconinck B, Nathan Kutz J. Computing spectra of linear operators using the Floquet–Fourier–Hill method. *Journal of Computational Physics*. 2006 Nov;219(1):296-321. doi:10.1016/j.jcp.2006.03.020.
- [68] Jordan D, Smith P, Jordan D, Smith P. *Nonlinear Ordinary Differential Equations: An Introduction for Scientists and Engineers*. Fourth edition, fourth edition ed. Oxford Texts in Applied and Engineering Mathematics. Oxford, New York: Oxford University Press; 2007.
- [69] Inc WR. *Mathematica, Version 14.0*; Champaign, IL, 2024.

Appendices

App. A Pseudospectral method to integrate Eq. (2.4).

We performed the numerical simulations of Eq. (2.1) and (2.4) using a pseudospectral integration method on a spatial grid with periodic boundary conditions, cell size Δx and time step Δt . The basis of the pseudospectral method is to split a given partial differential equation (PDE), such as (2.4), into a linear and a nonlinear part

$$\partial_t \rho = \mathcal{L} \rho + \mathcal{N}(\rho(\mathbf{x}, t)), \quad (\text{A.1})$$

where \mathcal{L} are the linear terms and $\mathcal{N}(\rho(\mathbf{x}, t))$ the non-linear terms. Upon writing the PDE in this way, we can apply the spatial Fourier transform \mathcal{F} to Eq. (A.1) to get

$$\partial_t \hat{\rho}(\mathbf{k}, t) = \alpha(\mathbf{k}) \hat{\rho}(\mathbf{k}, t) + \Phi(\hat{\rho}(\mathbf{k}, t)) \quad (\text{A.2})$$

where $\hat{\rho}(\mathbf{k}, t) = \mathcal{F}[\rho(\mathbf{x}, t)]$, $\alpha(\mathbf{k})$ is the Fourier transform of the linear operator \mathcal{L} , and $\Phi(\mathbf{k}, t) = \mathcal{F}[\mathcal{N}(\mathcal{F}^{-1}[\hat{\rho}(\mathbf{k}, t)])]$.

In the final step of the algorithm, we perform the numerical integration of Eq (A.2) using a fourth-order Runge Kutta method (RK4), such that in each time step Δt we apply the backward Fourier transform to the population density field $\hat{\rho}$ and save the configuration. The Python code with the implementation of the algorithm is available at [GitHub](#)

App. B Linear stability analysis of the nonlocal logistic model with a sine flow

To perform the linear stability analysis of the nonlocal logistic model with a sine flow [Eqs. (2.8)-(2.9) with $m = 1$], we first linearize Eq. (2.4) around the uniform configuration assuming a perturbed solution $\rho(\mathbf{u}, \tau) = \rho_0 + \epsilon \psi(\mathbf{u}, \tau)$ where $\rho_0 = \text{Da}$ is the uniform solution, and $\epsilon \ll 1$. This linearization gives an equation for the perturbation,

$$\frac{\partial \psi(\mathbf{u}, \tau)}{\partial \tau} = \nabla_{\mathbf{u}}^2 \psi(\mathbf{u}, \tau) - \text{Da} \int_E H(\mathbf{u} - \mathbf{v}) \psi(\mathbf{v}, \tau) d\mathbf{v} - \overline{\text{Pe}} \sin(\tilde{q} v) \frac{\partial \psi(\mathbf{u}, \tau)}{\partial u}. \quad (\text{B.1})$$

Next, because the system is periodic, we write an ansatz for the perturbation using a Floquet

decomposition [67, 68]

$$\psi(\mathbf{u}, \tau) \equiv \psi_{\mathbf{k}}(\mathbf{u}, \tau) = e^{i\mathbf{k}\cdot\mathbf{u} + \lambda(\mathbf{k})\tau} \sum_n C_n(\mathbf{k}) e^{in\tilde{q}v}. \quad (\text{B.2})$$

Because we are using $m = 1$, the sine flow has the same periodicity as the system domain. and the Floquet expansion in Eq. (B.2) can be rearranged to become a simple Fourier expansion. Here, we keep this slightly more general formulation because it could be generalized without difficulty to $m > 1$. Inserting the ansatz in Eq.(B.2) into the linear equation for the perturbation, Eq. (B.1), we obtain the following four terms.

- For the time derivative, we get

$$\partial_\tau \psi = e^{i\mathbf{k}\cdot\mathbf{u} + \lambda(\mathbf{k})\tau} \sum_n \lambda(\mathbf{k}) C_n(\mathbf{k}) e^{in\tilde{q}v} \quad (\text{B.3})$$

- For the diffusion term,

$$\nabla_u^2 \psi(\mathbf{u}, \tau) = -e^{i\mathbf{k}\cdot\mathbf{u} + \lambda(\mathbf{k})\tau} \sum_n k_n^2 C_n(\mathbf{k}) e^{in\tilde{q}v}, \quad (\text{B.4})$$

where we have defined $\mathbf{k}_n = (k_u, k_v + n\tilde{q})$ and $k_n = |\mathbf{k}_n|$.

- For the nonlocal competition term, the convolution becomes

$$\int_E H(\mathbf{u} - \mathbf{v}) \psi(\mathbf{v}, \tau) d\mathbf{v} = e^{i\mathbf{k}\cdot\mathbf{u} + \lambda(\mathbf{k})\tau} \sum_n \hat{H}(k_n) C_n(\mathbf{k}) e^{in\tilde{q}v}. \quad (\text{B.5})$$

- Finally, we can compute the advection term by expanding the sine function in the Euler notation and renaming the index n in the summatory. This procedure leads to

$$\overline{\text{Pe}} \sin(\tilde{q}v) \frac{\partial \psi(\mathbf{u}, \tau)}{\partial u} = \frac{\overline{\text{Pe}}}{2} k_u e^{i\mathbf{k}\cdot\mathbf{u} + \lambda(\mathbf{k})\tau} \sum_n [C_{n+1}(\mathbf{k}) - C_{n-1}(\mathbf{k})] e^{in\tilde{q}v} \quad (\text{B.6})$$

Collecting all these terms, we obtain an infinite-dimension system of coupled equations for the coefficients $C_n(\mathbf{k})$

$$\left[\lambda(\mathbf{k}) + k_n^2 + \nu \hat{H}(k_n) \right] C_n(\mathbf{k}) = k_u \frac{\overline{\text{Pe}}}{2} [C_{n+1}(\mathbf{k}) - C_{n-1}(\mathbf{k})]. \quad (\text{B.7})$$

Notice that, for $\overline{\text{Pe}} = 0$, this system of equations (B.7) reduces to the expression we obtained for

$\lambda(k)$ in the absence of flow,

$$\lambda(k) = -k^2 - \text{Da} \tilde{H}(k) \quad (\text{B.8})$$

Evaluating this limit case, we can obtain Da_c by computing the value of this parameter at which the maximum of $\lambda(k)$ becomes positive (cyan dashed line in Fig. A2). Remarkably, we obtain the same expression (B.8) if $k_u = 0$, which corresponds to perturbations with the shape of horizontal stripes. This means that when increasing Da we will find a pattern forming instability to stripes when $\text{Da} = \text{Da}_c$, the critical Damköhler value in the absence of flow. We can further investigate Eq. (B.7) to check if other instabilities appear at lower values of Da.

To reduce the dimensionality of this system, we consider the low- $\overline{\text{Pe}}$ limit by truncating the sum in n at $n = \pm 1$ (i.e., we assume that $C_n = 0 \forall |n| \geq 2$). This reduced system can be written in a matrix form as

$$\begin{pmatrix} \lambda(\mathbf{k}) + A(k_{-1}) & -B & 0 \\ B & \lambda(\mathbf{k}) + A(k_0) & -B \\ 0 & B & \lambda(\mathbf{k}) + A(k_1) \end{pmatrix} \begin{pmatrix} C_{-1}(\mathbf{k}) \\ C_0(\mathbf{k}) \\ C_1(\mathbf{k}) \end{pmatrix} = 0 \quad (\text{B.9})$$

with $A(k_n) = k_n^2 + \nu \hat{H}(k_n)$ and $B = k_u \overline{\text{Pe}}/2$. The eigenvalues of the matrix of coefficients in Eq. (B.9) can be computed analytically from its determinant. Its expressions, however, involve the sum of several Bessel functions with shifted arguments. We obtained them using Mathematica [69] and computed the Da value at which the maximum of the real part of the largest eigenvalue becomes positive. As shown in Fig. A2, this critical value of Da is the same we obtained in the absence of flow, which indicates that the sine flow has no effect on determining the pattern instability. This is consistent with the results of the nonlinear numerical simulations, which confirm that the homogeneous solution remains stable for $\text{Da} < \text{Da}_c$.

App. C Supporting Figures

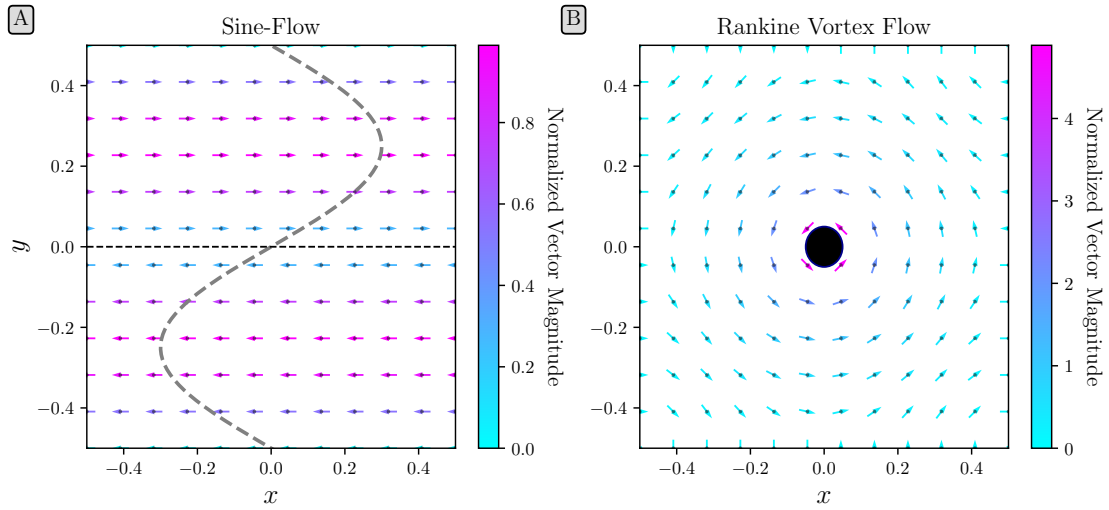


Figure A1: Vector field of the (A) sine and (B) Rankine vortex flow. The arrows indicate the direction of the flow and the intensity is given by the color as indicated in each panel's colorbar. The central black disk in B marks the region where velocity increases linearly with distance to the vortex center (placed at the center of the simulation domain).

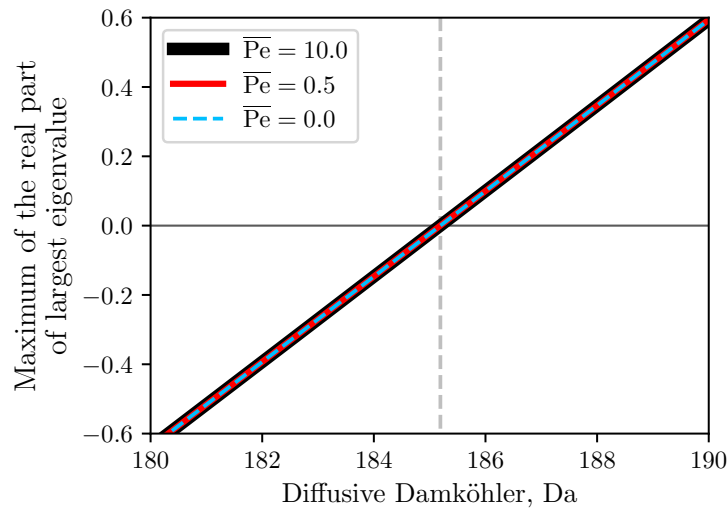


Figure A2: Maximum of the real part of the largest eigenvalue as a function of Da for the non-flow system and two different values of \overline{Pe} . The gray-dashed vertical line indicates the value of Da_c .

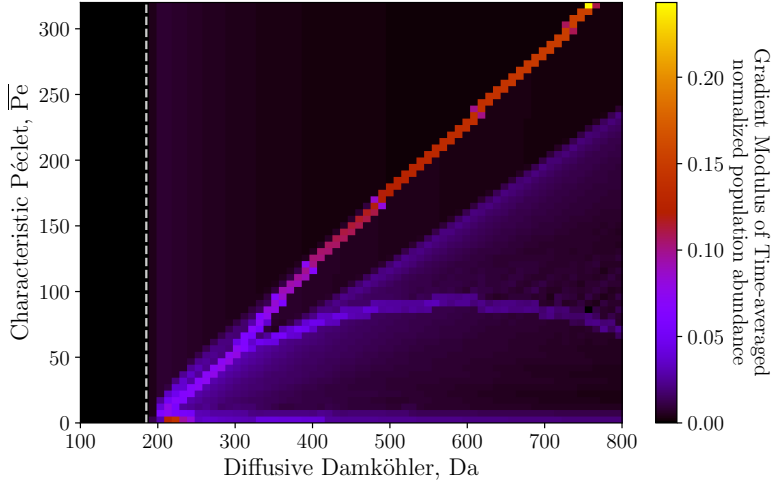


Figure A3: Sine flow. The modulus of the gradient of the time-averaged population abundance with respect to Da and \overline{Pe} captures the transitions between pattern shapes and allows us to define sub-regions in the parameter space with qualitatively similar spatiotemporal population dynamics. The white dashed line indicates the value of the Damköhler number Da_c at which patterns first form in the absence of flow.

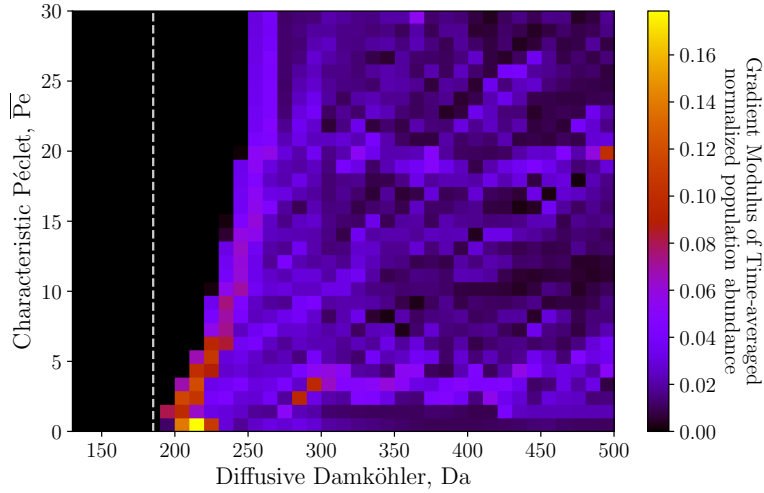


Figure A4: Rankine vortex. The modulus of the gradient of the time-averaged population abundance with respect to Da and \overline{Pe} does not capture the transitions between pattern shapes and hence does not allow us to define sub-regions in the parameter space with qualitatively similar spatiotemporal population dynamics. The white dashed line indicates the value of the Damköhler number Da_c at which patterns first form in the absence of flow.